REPUBLIC OF TURKEY

YILDIZ TECHNICAL UNIVERSITY

GRADUATE SCHOOL OF NATURAL AND APPLIED SCIENCES

DESIGN AND IMPLEMENTATION OF MULTI-AXIS INDUCTIVE DISPLACEMENT SENSOR

Yunus Emre TOMRUK

MASTER OF SCIENCE THESIS

Department of Mechatronics Engineering

Mechatronics Engineering Program

Advisor

Assoc. Prof. Kadir ERKAN

December, 2019

REPUBLIC OF TURKEY

YILDIZ TECHNICAL UNIVERSITY

GRADUATE SCHOOL OF NATURAL AND APPLIED SCIENCES

DESIGN AND IMPLEMENTATION OF MULTI-AXIS INDUCTIVE DISPLACEMENT SENSOR

A thesis submitted by Yunus Emre TOMRUK in partial fulfilment of the requirements for the degree of MASTER OF SCIENCE is approved by the committee on 06.12.2019 in Department of Mechatronics Engineering, Mechatronics Engineering Program.

Assoc. Prof. Kadir Erkan
Yıldız Technical University
Advisor

Approved by the Examining Committee

Assoc. Prof Kadir Erkan, Advisor
Yıldız Technical University _____

Assoc. Prof. Cüneyt Yılmaz, Member
Yıldız Technical University _____

Asst. Prof. Korhan Kayışlı, Member
Nişantaşı University _____

I hereby declare that I have obtained the required legal permissions during data collection and exploitation procedures, that I have made the in-text citations and cited the references properly, that I haven't falsified and/or fabricated research data and results of the study and that I have abided by the principles of the scientific research and ethics during my Thesis Study under the title of Design And Implementation of Multi-Axis Inductive Displacement Sensor supervised by my supervisor, Assoc. Prof. Kadir ERKAN. In the case of a discovery of false statement, I am to acknowledge any legal consequence.

Yunus Emre TOMRUK

Signature

Dedicated to my family

ACKNOWLEDGEMENTS

I would like to thank my advisor Mr. ERKAN for his support and encouragement and Mr. GUNEY for his guidance during the processes.

I also would like to thank the ALTINAY Aerospace and Advanced Technologies family.

Yunus Emre TOMRUK

TABLE OF CONTENTS

LIST OF SYMBOLS 6

LIST OF ABBREVIATIONS 7

LIST OF FIGURES 8

LIST OF TABLES 10

ABSTRACT 11

ÖZET 13

1 Introduction 15

1.1 Literature Review 15

1.2 Objective of the Thesis 21

1.3 Hypothesis 21

2 Electromagnetic Analysis 22

2.1 System Description 22

2.1.1 Analytical Model Development 24

2.1.2 Analytical Solution Results 28

2.1.3 3D Finite Element Analysis 32

3 Experimental Setup 38

3.1 Test Results 40

4 Results And Discussion 46

APPENDIX A 48

APPENDIX B 54

APPENDIX C 56

References 57

Publications from the thesis 59

LIST OF SYMBOLS

T	Tesla
N	Number of Turns
t	Coil Thickness
e	EMF
φ	Flux
i	Current
R_{gap}	Air Gap Reluctance
P_{gap}	Air Gap Permeance
μ_0	Relative Permeability of Air
l	Core Length
μ_{rc}	Relative Permeability of Core Material
μ_{rt}	Relative Permeability of Target Material
A	Cross-section Area of the Coils
f	Excitation Frequency
z	Linear Displacement of The Target
α	Angle Change Between Target and Sensing Coils Thorough X Axis
β	Angle Change Between Target and Sensing Coils Thorough Y Axis
V	Induced Voltage

LIST OF ABBREVIATIONS

3D	3 Dimensions
SMM	Soft Magnetic Material
SMC	Soft Magnetic Composite
IC	Integrated Circuit
ECS	Eddy Current Sensor
PCB	Printed Circuit Board
AMB	Active Magnetic Bearing
VR	Variable Reluctance
EMF	Electromotive Force

LIST OF FIGURES

Figure 1.1 A single axis eddy current sensor by Ragunathan, P et al. 16

Figure 1.2 (a) Conceptual illustration of front-end stage in the proposed ECS interface; (b) simplified block diagram of the implemented sensor interface (x: distance between coil and target) by M. R. Nabavi. 17

Figure 1.3 Simplified diagram of the proposed inductive displacement sensor by B. Anish and G. Boby 17

Figure 1.4 Single coil printed circuit based inductive displacement sensor by O. Sosnicki et al. 18

Figure 1.5 Inductive sensor head position, (a) radial sensors; (b) axial sensors; (c) experimental setup by Chen, Seng et al. 18

Figure 1.6 The inductive displacement sensor block diagram by R. Luigi and C. Stefano 18

Figure 1.7 PCB flux-gate sensor by L. Rovati and S. Cattini 19

Figure 1.8 PCB flux-gate sensor by P. Reddy et al. 19

Figure 1.9 Presented IC and sensing circuit by P. Reddy et al. 20

Figure 1.10 PCB eddy current displacement sensor by Grobler, A.J. et al. 20

Figure 2.1 Sensor structure 22

Figure 2.2 Sensor dimensions 23

Figure 2.3 Equivalent circuit 26

Figure 2.4 Equivalent reluctance change of coils against displacement 30

Figure 2.5 Induced voltage against linear displacement 30

Figure 2.6 Equivalent reluctance vs tilt angle 31

Figure 2.7 Induced voltage vs tilt angle 32

Figure 2.8 Meshed structure 33

Figure 2.9 Target orientations 33

Figure 2.10 Magnetic flux distribution, isometric view 34

Figure 2.11 Magnetic flux distribution, side view 35

Figure 2.12 Excitation current 35

Figure 2.13 FEA result, induced voltage vs linear displacement 36

Figure 2.14 Comparison of FEA and analytical results, induced voltage vs linear displacement 37

Figure 2.15 Comparison of FEA and analytical results, induced voltage vs tilt angle 37
Figure 3.1 Sensor core AISI 430F stainless steel 38
Figure 3.2 The sensor built for experimental tests 39
Figure 3.3 Experimental setup 39
Figure 3.4 Test results, induced voltage vs linear displacement 43
Figure 3.5 Tilt change of target, exaggerated illustration 43
Figure 3.6 Test results, induced voltage vs tilt angle 45
Figure A.1 Simulink model of equivalent circuit 53
Figure B.1 Magnetic properties 54
Figure B.2 Somalloy Magnetic properties 54
Figure C.1 Sensor core technical drawing 56

LIST OF TABLES

Table 2.1 Sensor parameters for number of turns of 49 24
Table 2.2 Reluctance parameters 27
Table 2.3 Parameter used in calculations 29
Table 2.4 Mesh parameters 33
Table 3.1 The built sensor parameters 40
Table 3.2 Test parameters 40
Table 3.3 Test results, induced voltage (peak to peak) vs linear displacement 42
Table 3.4 Test results, induced voltage (peak to peak) vs tilt angle 44
Table B.1 430F material properties 54

ABSTRACT

DESIGN AND IMPLEMENTATION OF MULTI-AXIS INDUCTIVE DISPLACEMENT SENSOR

Yunus Emre TOMRUK

Department of Mechatronics Engineering

Master of Science Thesis

Advisor: Assoc. Prof. Kadir ERKAN

In this study a novel multi axis inductive displacement sensor designed and analysed by analytical and 3D finite elements method. The proposed sensor capable to measure the displacement of the objects without contact, and it can also be used for tilt angle measurement applications. A novel structure has one excitation coil in the middle of the square base and four sensing coils at the corners. This structure allows us to sense the tilt on the target metal by evaluating the voltage changes on the sensing coils. The sensor core is made from soft magnetic material, and it allows us to excite the sensor coil with high frequencies because the material's magnetic characteristic significantly decreases eddy current losses. To prevent the skin effect steel target thickness have chosen as 5mm in the analysis. First, an analytical model is developed to express the measurement process and then 3D finite element analysis is performed to verify analytical model by using Ansys Maxwell software. In the analysis 0-5mm linear movement is considered. Then the tilt measurements executed between 0-3° at 1mm distance, and the results show that the changes on two of the sensing coils are linearly decreasing while the voltage on other two sensing coil linearly increasing. Finally, the sensor is built and experiments are performed.

Key Words: Inductive sensor, tilt angle, displacement measurement

ÖZET

ÇOK SERBESTLİK DERECELİ ENDÜKTİF MESAFE SENSÖRÜ TASARIMI VE UYGULAMASI

Yunus Emre TOMRUK

Mekatronik Mühendisliği Bölümü

Yüksek Lisans Tezi

Danışman: Doç Dr. Kadir ERKAN

Bu çalışmada özgün çok eksenli endüktif yer değiştirme sensörü tasarlanmış, analitik ve sonlu elemanlar yöntemleri kullanılarak analiz edilmiştir. Bu çalışmada önerilen sensör, metal nesnelerin sensör bobinleri ile arasındaki doğrusal mesafenin ve eğim açılarının nesneye temas etmeden ölçülebilmesini sağlamaktadır. Sensör kare bir taban üzerine oturtulmuş bir adet uyartım bobini(ortada) ve dört adet algılama bobinlerinden(köşelerde) oluşmaktadır. Bu yapı, algılama bobinlerindeki voltaj değişikliklerinin değerlendirilerek hedefin sensöre olan uzaklığı ve sensör ile yaptığı eğim açısını algılamamıza olanak sağlar. Sensör çekirdeği yumuşak manyetik malzemeden üretilmiştir, bu malzemenin manyetik özelliği sayesinde girdap akım kayıpları önemli ölçüde azaltılır ve bu da bize sensör bobinini yüksek frekanslarda uyartabilme imkanı sağlar. Deri etkisini önlemek için çelik hedef kalınlığı analizde 5 mm olarak seçilmiştir. İlk olarak sensör analitik modeli geliştirilmiştir, ardından Ansys Maxwell yazılımı kullanılarak 3B sonlu elemanlar analizi yapılmış ve sonuçlar değerlendirilmiştir. Analiz hedefin 0-5mm doğrusal hareket ettiği durum için gerçekleştirilmiştir. Hedefin eğim açısının sensör üzerindeki etkisi hedefin sensöre 1 mm mesafede konumlandırıldığı ve açı değişiminin tek eksende 0-3° arasında gerçekleştiği durum için gerçekleştirilmiştir. Sonuç olarak açı değişiminde hedefin yakın

kenarında kalan iki bobinde endüklenen gerilimin doğrusal olarak arttığı diğer tarafta kalan bobinlerde ise doğrusal olarak azaldığı görülmüştür. Son olarak sensör üretilmiş ve deneysel çalışmalar gerçekleştirilmiştir.

Anahtar Kelimeler: Endüktif sensör, eğim açısı, doğrusal yerdeğişimi ölçümü

1 Introduction

1.1 Literature Review

With developing technology, the need for accurate position and/or displacement measurements in the micro meter level has increased significantly. In the industry, different type of applications about position and displacement sensing can be found. For many of these, sensors based on mechanical contact are sufficient to position measurements, but some of these applications are require non-contact measurement. Some of these applications and their features are as follows;

Air Gaugin: These devices operate on changes in pressure and flow rates to make a measurement. [1] Pressure and flow rate are directly proportional to the clearance so as clearance increases air flow also increases, and air pressure decreases proportionately. As clearance decreases, air flow also decreases, and air pressure increases.

Hall Effect: This sensor measures the changes in magnetic field by evaluating the varying output voltage on the sensor.

Ultrasonic: Ultrasonic sensors operate on a principle similar to sonar by interpreting echoes of sound waves reflecting off a target. [1]

Photonic: Photonic sensors use glass fibers to transmit light to and from target surfaces. Displacement is determined by detecting the intensity of the reflected light. [1]

Capacitance: These sensors work on the principal of capacitance changes between the sensor and target to determine distance. They can be used with all conductive target materials and are not sensitive to material changes.

Inductive: Inductive sensors operates on the principle of Faraday law. Any change in the magnetic environment of a coil of wire will cause a voltage (emf) to be "induced" in the coil. Some of these sensor uses directly this phenomena and others measures the impedance variation caused by eddy currents induced in a conductive target by a sensor coil. [1]

Since magnetic fields are not sensitive to the presence of contaminants such as oil, dirt, dust, etc., the inductive sensors operate well even in polluted environments and widely used for contactless measurement. [2-5].

In the literature, many kinds of measurement applications were investigated using inductive sensors for displacement and proximity sensing [5-13]. Studies on inductive measurement can be classified as follows; [4]

- By sensing principle; inductive and eddy current.
- By sensor structure; air coil, coils with ferromagnetic cores, flat coils, pcb coils and some hybrid structures.
- Sensor interfaces.

In detail, the studies mostly focused on improving thermal stabilities, sensing range, measurement quality and resolution of the sensors. [5-8,12,13]

Some of the studies about eddy current and inductive sensors are presented as follows;

[14] presents a design method and fabrication of a low-cost single coil eddy current sensor used in real time servo-control feed-back in active magnetic bearing which is a coil of wire near the end of the sensor probe. A single axis magnetic bearing system showing the magnetic coil, levitated steel bolt and eddy current position sensor shown in the Figure 1.1.



Figure 1.1 A single axis eddy current sensor by Ragunathan, P et al.

[2] focusses on developing an IC interface for eddy current sensor. At first, he mentions the imperfections of eddy current sensors such as penetration depth δ, mechanical instabilities and sensitivity of the ECS to stray magnetic fields, to find the optimum solution.

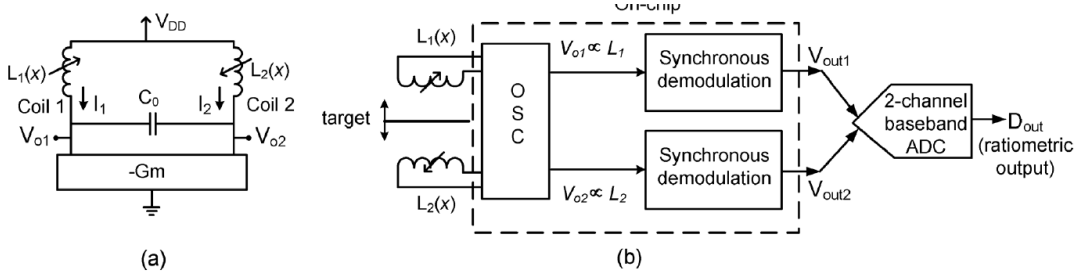


Figure 1.2 (a) Conceptual illustration of front-end stage in the proposed ECS interface; (b) simplified block diagram of the implemented sensor interface (x: distance between coil and target) by M. R. Nabavi.

At [15] a new, non-contact, planar spiral coil based inductive displacement sensor is presented. The proposed sensor employs a fixed planar coil and a movable U-shaped magnetic core. . The planar coil PCB is the fixed part of the sensor, while the U-core travels along with the measurand x. To achieve higher displacement range, the PCB can be extended using additional identical planar coil and electrodes.

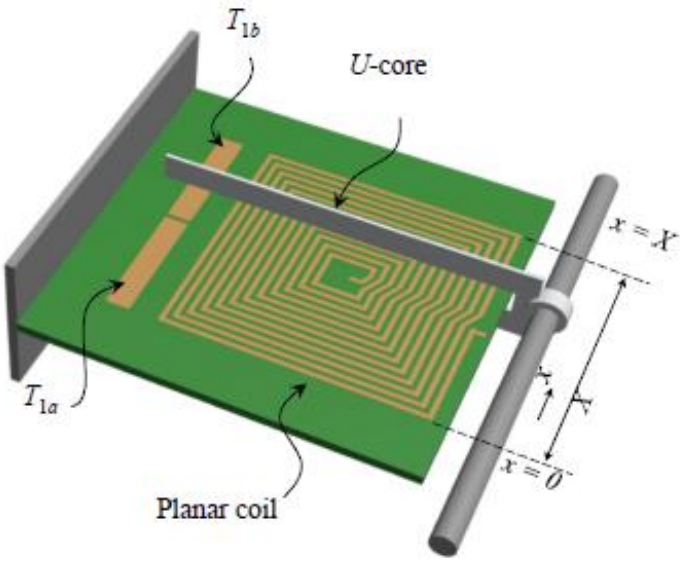


Figure 1.3 Simplified diagram of the proposed inductive displacement sensor by B. Anish and G. Boby

In [16] the modelling of the magnetic behaviour of the pcb eddy current sensor with dedicated electronic conditioning are studied.

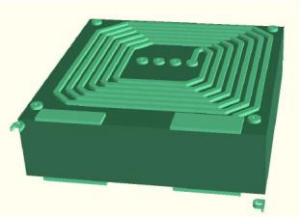


Figure 1.4 Single coil printed circuit based inductive displacement sensor by O. Sosnicki et al.

In [17], the differential inductive sensor head and lock-in amplifier for synchronous demodulation, designed. In addition, an active low-pass filter and a notch filter were used to eliminate disturbances, which caused by natural frequencies.

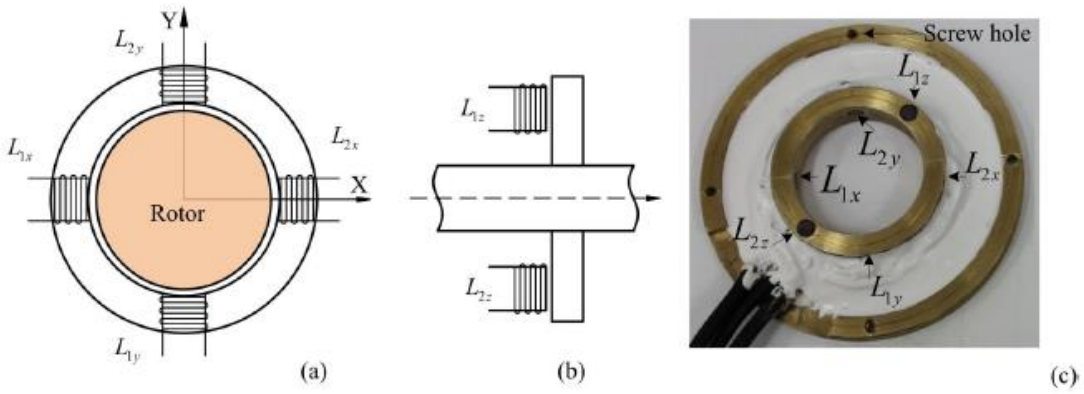


Figure 1.5 Inductive sensor head position, (a) radial sensors; (b) axial sensors; (c) experimental setup by Chen, Seng et al.

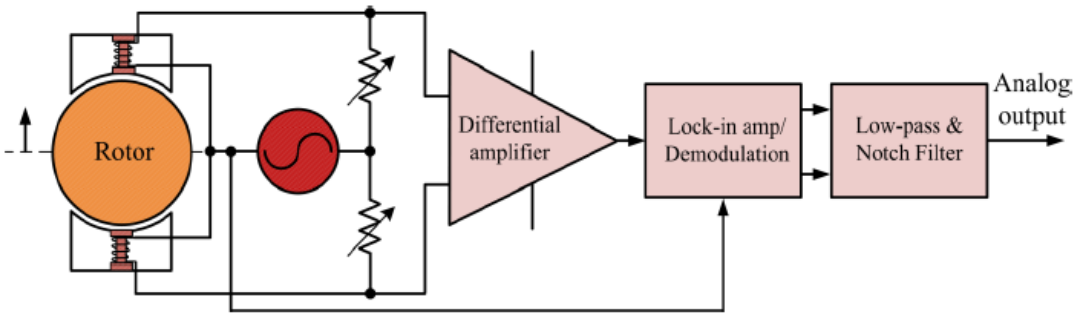


Figure 1.6 The inductive displacement sensor block diagram by R. Luigi and C. Stefano.

In [18] a tilt sensitive measuring system that exploits two magnets and a flux-gate sensor to measure two axis tilt is presented. The sensing configuration has been investigated and the prototype characterization is shown. It consists of an excitation coil, four sensing coils, and a ferromagnetic x-shaped core. The green coil represents the excitation coil

providing the excitation field HEX, the grey parallelepiped represents one arm of thin x-shaped core, and the red coils represent the relative two sensing coils sensitive to axial component of the external field B0. [10]

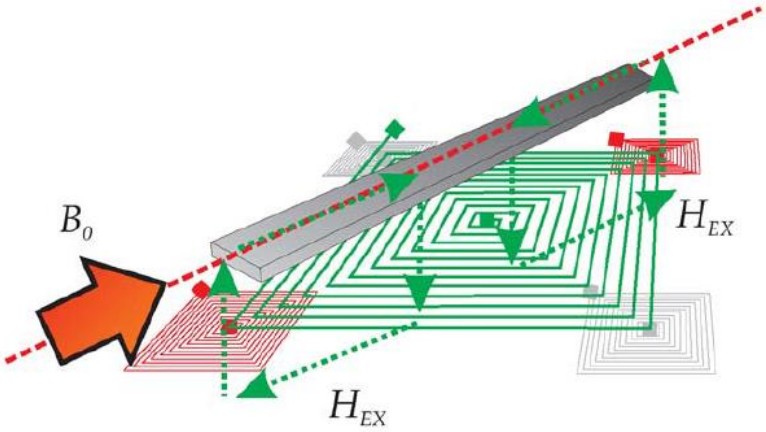


Figure 1.7 PCB flux-gate sensor by L. Rovati and S. Cattini

Another study proposes [19] a new contactless variable reluctance (VR) resolver that can be built on a PCB as coil traces. The coil layout consists of an excitation coil and two sense coils laid on a single plane of a PCB. It also presents a special sensor interface for the application.

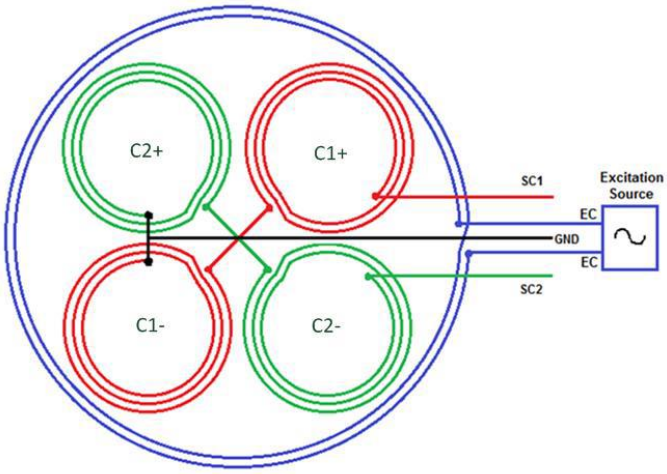


Figure 1.8 PCB flux-gate sensor by P. Reddy et al.

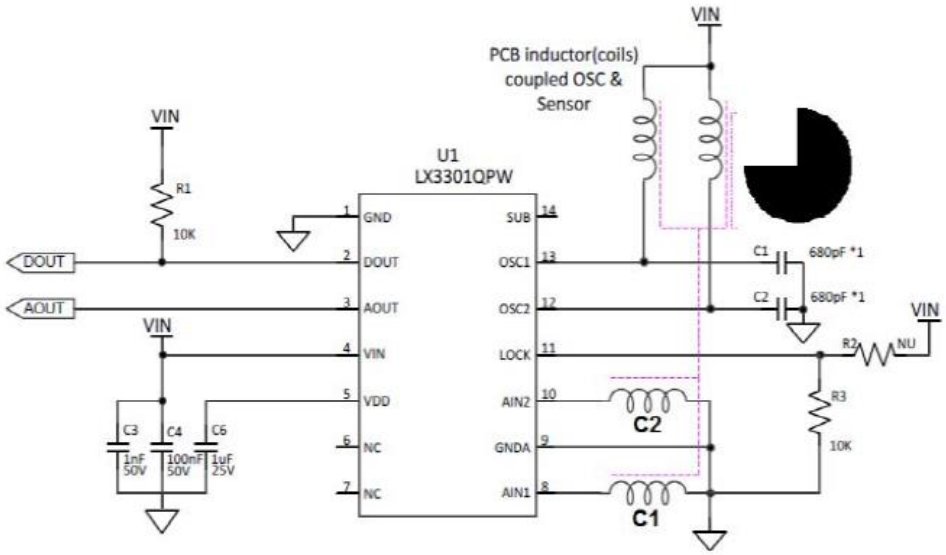


Figure 1.9 Presented IC and sensing circuit by P. Reddy et al.

In [20] a low cost pcb position sensor is presented. The sensor magnetic operation and the effects of the target material and the number of PCB layers are analyzed. Sensor structure is shown in the following figure.

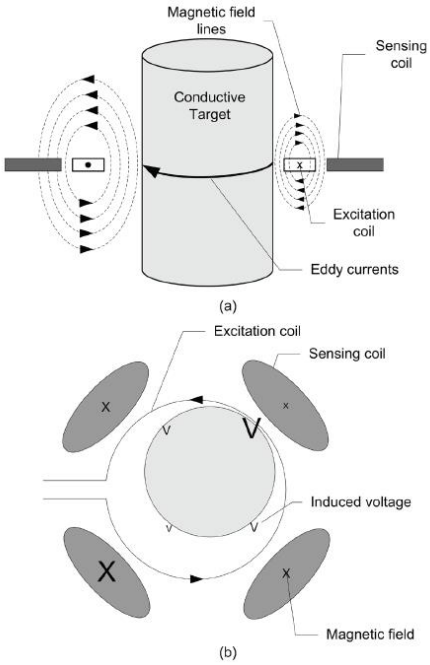


Figure 1.10 PCB eddy current displacement sensor by Grobler, A.J. et al.

1.2 Objective of the Thesis

Although some studies have done about angular measurement and tilt measurement as mentioned above and some others, there is no study about multi axis tilt angle measurement by using inductive displacement measurement principle. The objective of this study is to create contactless multi axis inductive displacement sensor.

1.3 Hypothesis

The novel approach of this study is to create contactless multi axis measurement by using inductive sensing principle. So, a sensor structure which have one excitation coil and four sensing coils is designed and analysed. Finally, sensor is built and tested. By evaluating the voltage changes on sensing coils caused by movement of target, displacement ant tilt angle measurement is performed.

2
Electromagnetic Analysis

2.1 System Description

A novel structure has one excitation coil in the middle of the square base and four sensing coils at the corners as shown in following figure. This structure allows us to sense tilt on the steel target by evaluating the voltage changes on the sensing coils. The sensor is excited by an excitation circuit which creates sine waves. That causes voltage induction on sensing coils. According the position of the target, induced voltage on sensing coils varies. By evaluating the voltage changes on sensing coils, we can find the exact position of the target.

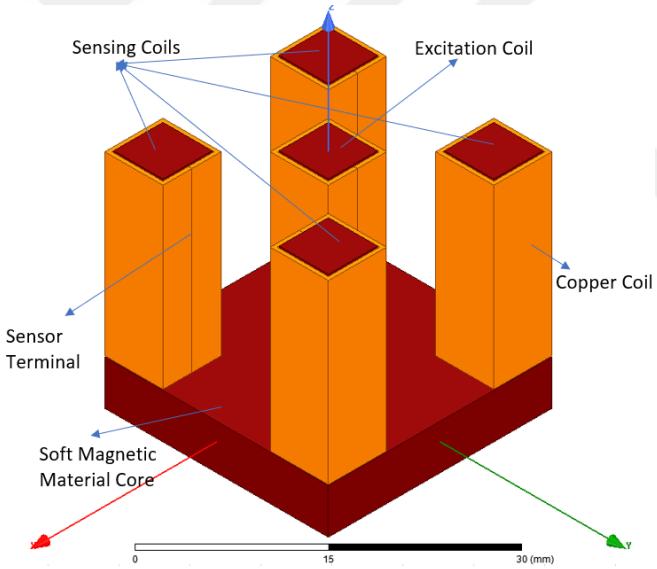


Figure 2.1 Sensor structure

This structure allows us to sense target position in multi degrees by evaluating voltage changes on sensing coils which are placed at corners. It also minimizes power consumption for such inductive measurement method due to minimizing excitation to one coil.

At first core material is defined. This is an important aspect because of we want to build a small sensor but have a wider range so we need relatively high excitation frequency[1Mhz]. And magnetic materials can be magnetized in relatively high

frequencies. Therefore, a soft magnetic material which is magnetic flux density greater than 1 T is chosen.

Sensor outline dimensions defined as 25x25x25mm to have relatively small sensor and coil dimensions designed as wide as possible to increase measurement range.

After defining dimensions copper wire length and number of turns defined as After defining dimensions copper wire length and number of turns defined as Table 3.1. While defining these parameters achieving high quality factor is aimed for having an ideal conductor.

The proposed sensor dimensions used for analysis are presented in below figure.

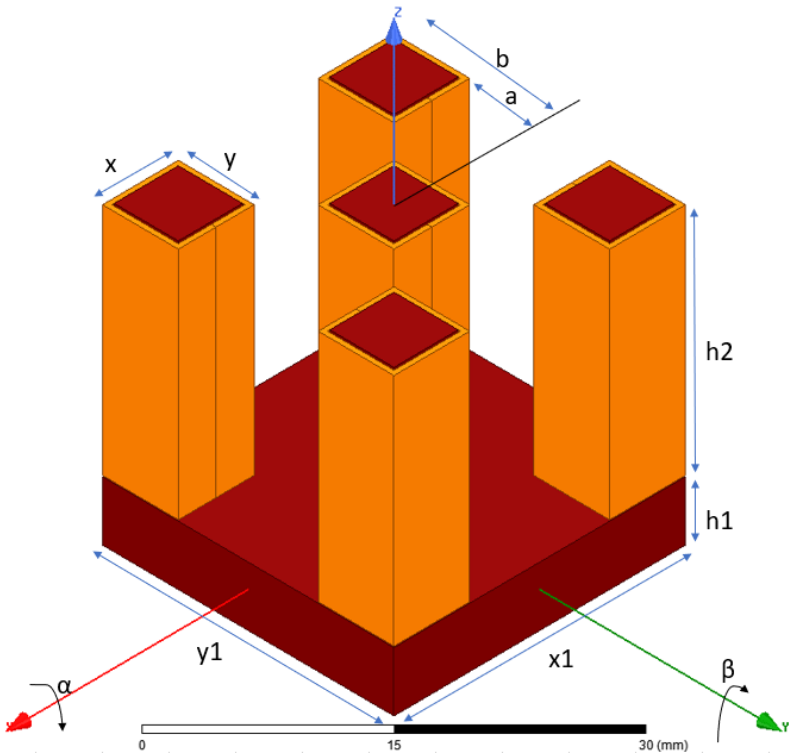


Figure 2.2 Sensor dimensions

Table 2.1 Sensor parameters for number of turns of 49

Parameter	Magnitude
t (Coil thickness)	0.4
x1	25
y1	25
h1	5
h2	20
x	6
y	6
a	6.5
b	12

2.1.1 Analytical Model Development

Any change in the magnetic environment of a coil of wire will cause a voltage (emf) to be "induced" in the coil. No matter how the change is produced, the voltage will be generated. The change could be produced by changing the magnetic field strength, moving a magnet or metal toward or away from the coil, moving the coil into or out of the magnetic field, rotating the coil relative to the magnet, etc. says Faraday's law and presents this phenomenon as follows;

$$e = -N\frac{d\phi}{dt} \tag{2.1}$$

where, N is the number of turns of the coil, ϕ is magnetic flux and expressed as follows by assuming the magnetic resistance and the hysteresis of the sensor core, eddy currents, flux leakage and fringing effects are neglected;

$$\phi = \frac{Ni}{R_{gap}} \tag{2.2}$$

where, i is the excitation current and R_{gap} is the reluctance of airgap between sensor head and target can be calculated as follows;

$$R_{gap} = \frac{x}{\mu_0 s} \tag{2.3}$$

where, x is length of the airgap, μ is the permeability and S is the pole cross section area. Permeance can be defined as inverse of reluctance.

Permeance values change by linear displacement and tilt angle of target represented as *z, α, β*. These permeances can be calculated by solving double-integrals as follows;

$$P_{gap1} = \int_{a}^{b} \int_{-b}^{-a} \frac{\mu_0}{z - tan\beta + xtan\alpha} dx\, dy \tag{2.4}$$

$$P_{gap2} = \int_{-b}^{-a} \int_{-b}^{-a} \frac{\mu_0}{z - tan\beta + xtan\alpha} dx\, dy \tag{2.5}$$

$$P_{gap3} = \int_{-b}^{-a} \int_{a}^{b} \frac{\mu_0}{z - tan\beta + xtan\alpha} dx\, dy \tag{2.6}$$

$$P_{gap4} = \int_{a}^{b} \int_{a}^{b} \frac{\mu_0}{z - tan\beta + xtan\alpha} dx\, dy \tag{2.7}$$

In this study, above mentioned magnetic circuit principle is used in order to derive induced voltages.

Magnetic circuit equivalent of the system can be seen from the Figure 2.3.

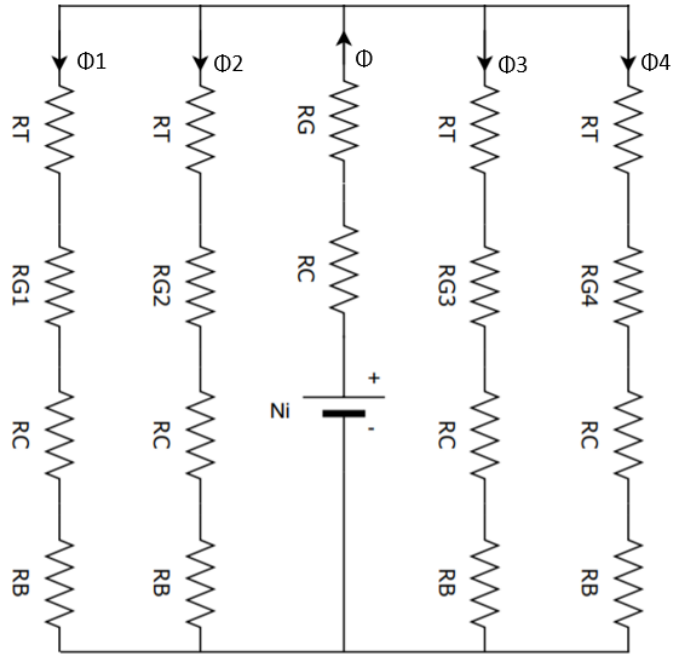


Figure 2.3 Equivalent circuit

RC, RB and RT are coil reluctance, core reluctance and target reluctance respectively and calculated as follows;

$$RC = \frac{l_c}{\mu_0 \mu_{rc} A_c} \tag{2.8}$$

$$RB = \frac{l_b}{\mu_0 \mu_{rb} A_b} \tag{2.9}$$

$$RT = \frac{l_t}{\mu_0 \mu_{rt} A_t} \tag{2.10}$$

Table 2.2 Reluctance parameters

Parameter	Magnitude	Unit
l_c	0.022	m
l_b	0.022	m
l_t	0.022	m
μ_0	$4x\pi x10^{-7}$	-
μ_{rc}	430	-
μ_{rb}	430	-
μ_{rt}	100	-
A_c	$30{,}25x10^{-6}$	m^2
A_b	$125x10^{-6}$	m^2
A_t	$125x10^{-6}$	m^2

From above equivalent circuit magnetic flux goes thorough excitation branch can be calculated as follows;

$$\phi = \frac{Ni}{R_{eq}} \tag{2.11}$$

where R_{eq} is the equivalent reluctance of the circuit and calculated as follows;

$$R_{eq} = RC + RG + \frac{1}{\frac{1}{R_1} + \frac{1}{R_2} + \frac{1}{R_3} + \frac{1}{R_4}} \tag{2.12}$$

and R_1, R_2, R_3 and R_4 are given expressed as below;

$$R_1 = RC+RB+RT+RG1 \tag{2.13}$$

$$R_2 = RC+RB+RT+RG2 \tag{2.14}$$

$$R_3 = RC+RB+RT+RG3 \tag{2.15}$$

$$R_4 = RC+RB+RT+RG4 \tag{2.16}$$

Magnetic fluxes go thorough other branches can be calculated as follows;

$$\phi_1 = \phi \frac{\frac{1}{\frac{1}{R_2}+\frac{1}{R_3}+\frac{1}{R_4}}}{R_1 + \frac{1}{\frac{1}{R_2}+\frac{1}{R_3}+\frac{1}{R_4}}} \tag{2.17}$$

$$\phi_2 = \phi \frac{\frac{1}{\frac{1}{R_1}+\frac{1}{R_3}+\frac{1}{R_4}}}{R_2 + \frac{1}{\frac{1}{R_1}+\frac{1}{R_3}+\frac{1}{R_4}}} \tag{2.18}$$

$$\phi_3 = \phi \frac{\frac{1}{\frac{1}{R_1}+\frac{1}{R_2}+\frac{1}{R_4}}}{R_3 + \frac{1}{\frac{1}{R_1}+\frac{1}{R_3}+\frac{1}{R_4}}} \tag{2.19}$$

$$\phi_4 = \phi \frac{\frac{1}{\frac{1}{R_1}+\frac{1}{R_2}+\frac{1}{R_3}}}{R_4 + \frac{1}{\frac{1}{R_1}+\frac{1}{R_3}+\frac{1}{R_4}}} \tag{2.20}$$

2.1.2 Analytical Solution Results

Induced voltage on each sensing coils are calculated by using Faraday's Law for parameters shown in Table 2.3 and results are presented in the following figures.

Table 2.3 Parameter used in calculations

Parameter	Magnitude	Unit
i (excitation current)	10	mA
f (excitation frequency)	1	MHz
N (number of turns)	49	-
z (linear displacement of the target)	0.2-5	mm
α (angle change between target and sensing coils thorough x axis)	0-3	◦
β (angle change between target and sensing coils thorough y axis)	0	◦

Analytical model built on MATLAB/Simulink environment and results are presented on following figures.

Figure 2.4 shows the equivalent reluctance change against linear displacement. Reluctance depend on linear and angular displacement, magnetic permeability of the core and target, and cross-sectional area of the sensing core. As we can see from (2.8) for a specific structure only distance between target and coil can affect the reluctance of a coil. And it is proportional to the linear displacement because there is no angular change on target.

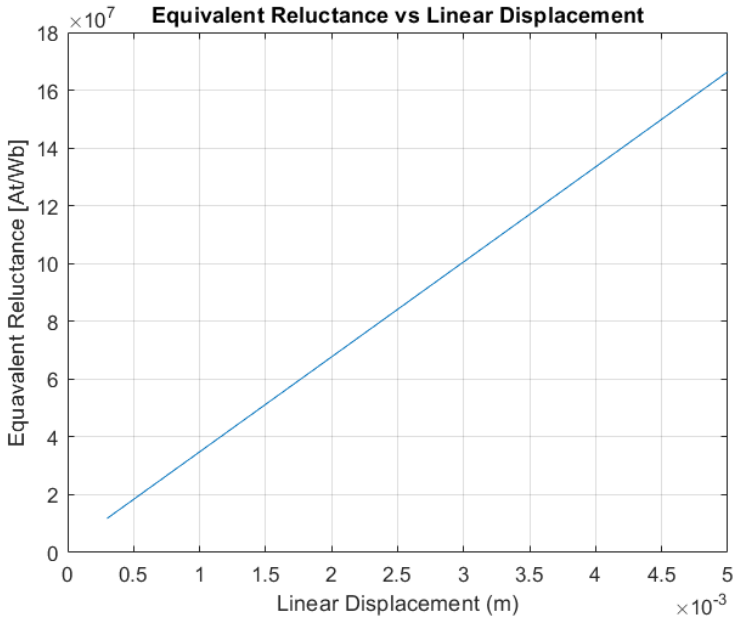


Figure 2.4 Equivalent reluctance change of coils against displacement

Figure 2.5 shows the induced voltage change against linear displacement of four sensing coil. Since four sensing coils are identical, the induced voltage on four sensing coils are also identical. Even though the equivalent reluctance is proportional to the linear displacement, the induced voltage is nonlinear because of the Faraday's Law.

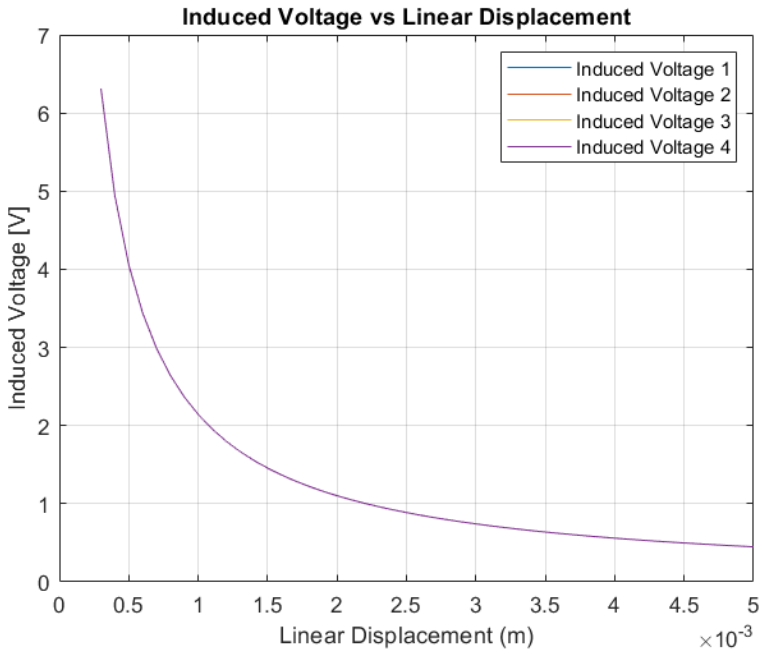


Figure 2.5 Induced voltage against linear displacement

Figure 2.6 shows the equivalent reluctance change against tilt angle. As shown in the figure it shows nonlinear behaviour. Because it's not only depended on point to point linear displacement. When a tilt occurs on the target, the area of the coils tracks on target changes and it creates a nonlinear change on the reluctance of the air gap and consequently equivalent reluctance as shown in the figure.

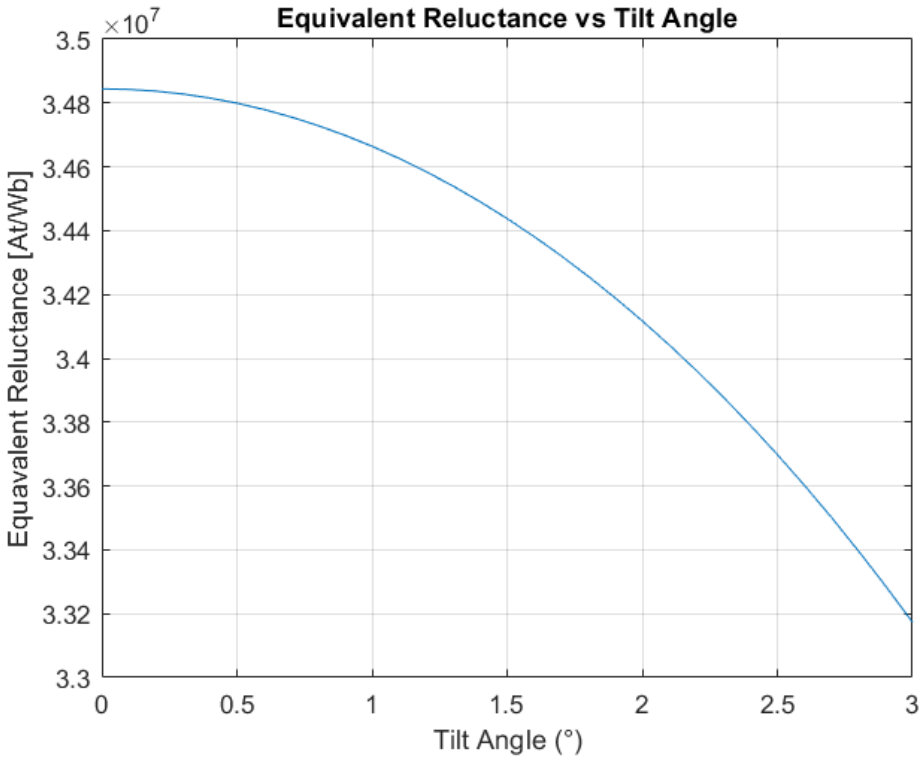


Figure 2.6 Equivalent reluctance vs tilt angle

Figure 2.7 shows the change the induced voltage on the sensing coils against tilt on target. It shows a linear change on coils but while the induced voltage on two of the coils are increasing, the voltage on other two coils are decreasing this is because of the while the target getting closer to the first two coils, it moves away from the other two.

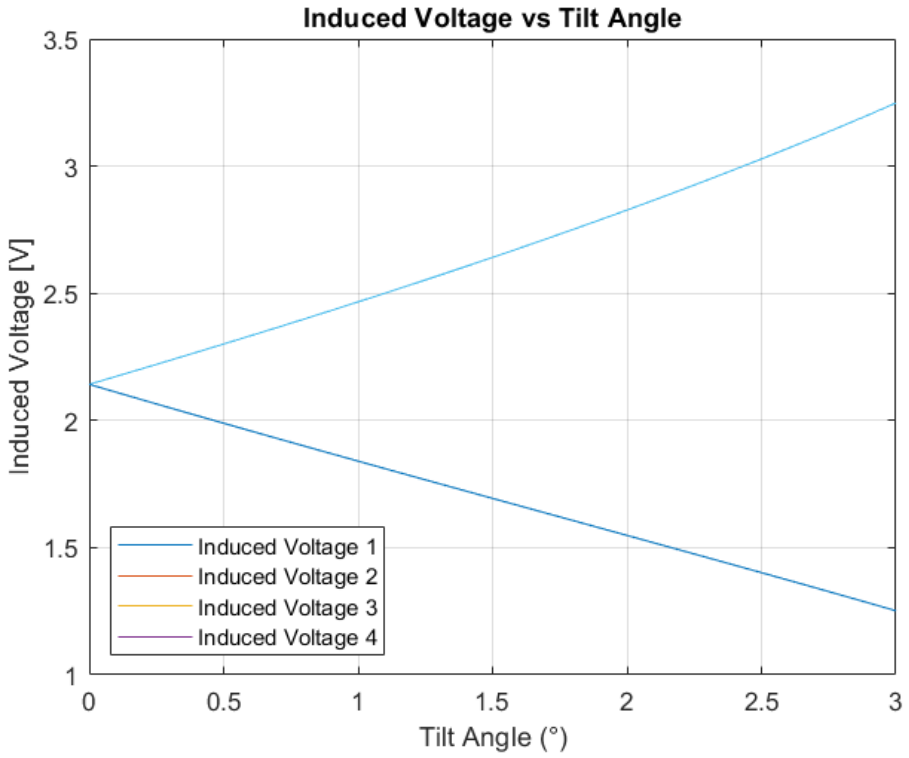


Figure 2.7 Induced voltage vs tilt angle

2.1.3 3D Finite Element Analysis

Finite element analysis performed by using Ansys Maxwell software and magnetic transient solver used. The magnetic transient solver computes time varying magnetic fields and solves for instantaneous magnetic fields at each time step. Before starting the analysis, model is designed on Ansys Maxwell. Core material is selected as Somalloy soft magnetic material, because its high flux density which allows us to work on high frequencies without magnetization. Coils are designed as solid copper which has 4mm thickness. Target material is selected as steel and to reduce eddy current effects and loses, target dimensions are selected as 50x50x5mm. Finally, 100x100x100mm vacuum space created around the sensor.

After completing the design, mesh operations are performed separately on core, coil and target. And mesh parameters are listed on the following table.

Table 2.4 Mesh parameters

Name	Number of Additional Elements
Body	3000
Coil	5000
Target	5000

Meshed distrubition on the sensor and the target is shown in the Figure 2.8.

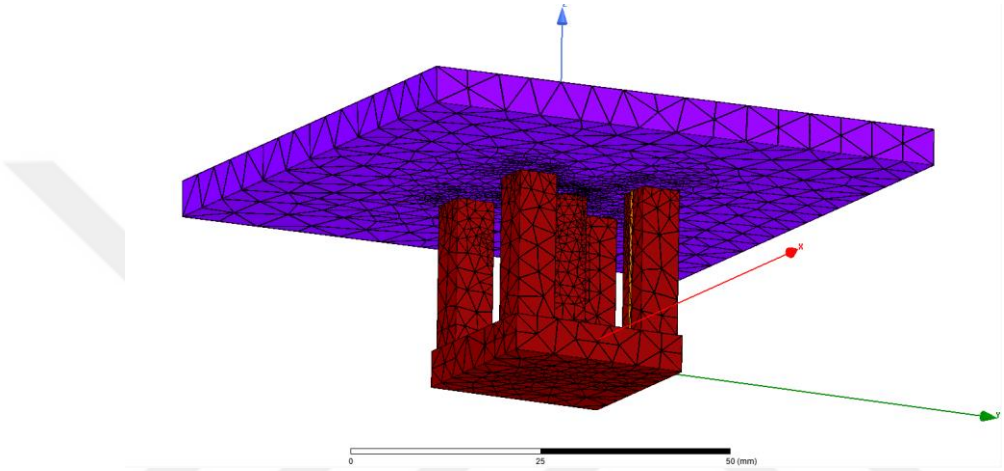


Figure 2.8 Meshed structure

Analysis performed for the linear and tilt movement of the target. These orientations are shown in Figure 2.9.

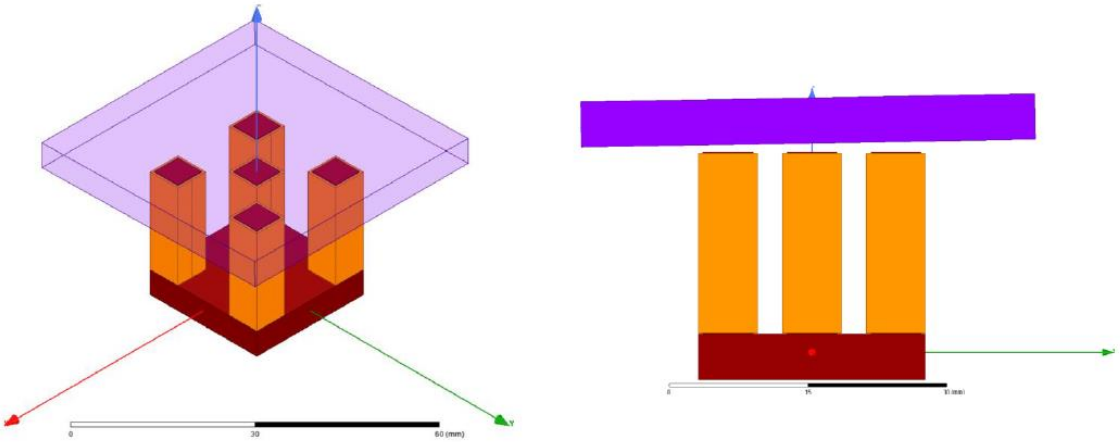


Figure 2.9 Target orientations

The transient solver requires specific information about the coil (such as the number of turns, parallel paths, and resistance) and the type of Excitation (Voltage, Current, or External). In general, Excitations thus require a definition of a Coil Terminal assignment, which is then assigned to Winding definition.

The coil terminal defines the direction of the current and number of conductors. In this application number of conductors defined as 49.

Winding definitions determine how coil are connected and the type of the source which is defined as current for this application. And excitation current defined as a function of time. Parameters are shown in Table 2.3. And excitation current is shown in Figure 2.12.

When the excitation coil is excited magnetic flux is created and starts to flow form excitation coil through target, sensing coils and the sensor core respectively. Magnetic flux density is maximum on the excitation coil as expected and lowers down while going through target and sensor core. Finally, it increases when completing to circuitry as seen in the Figure 2.10 and Figure 2.11.

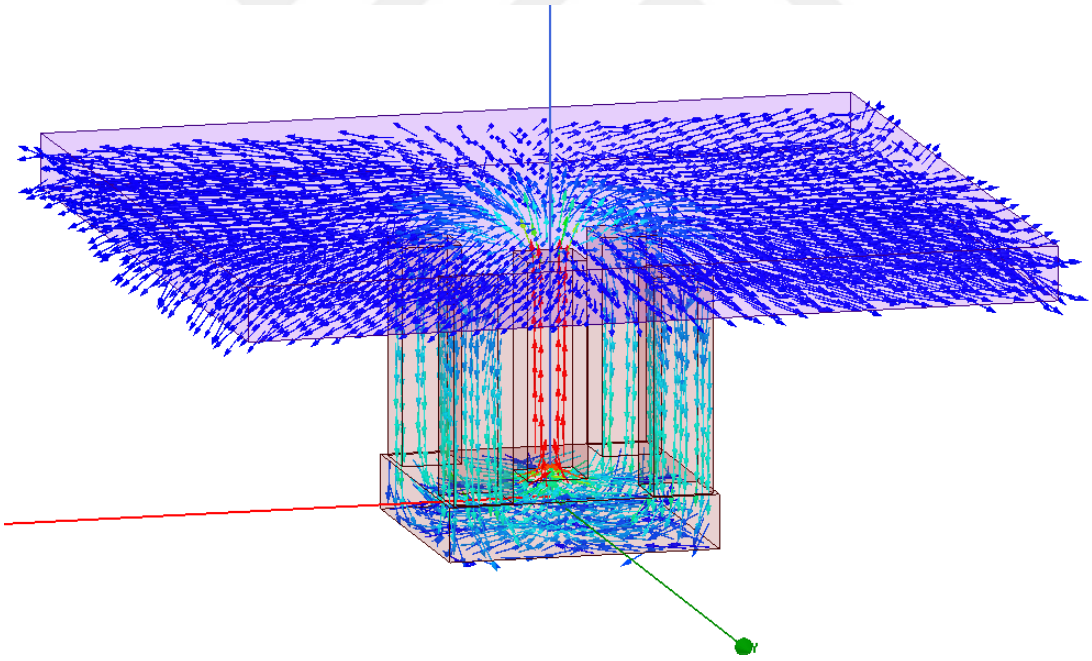


Figure 2.10 Magnetic flux distribution, isometric view

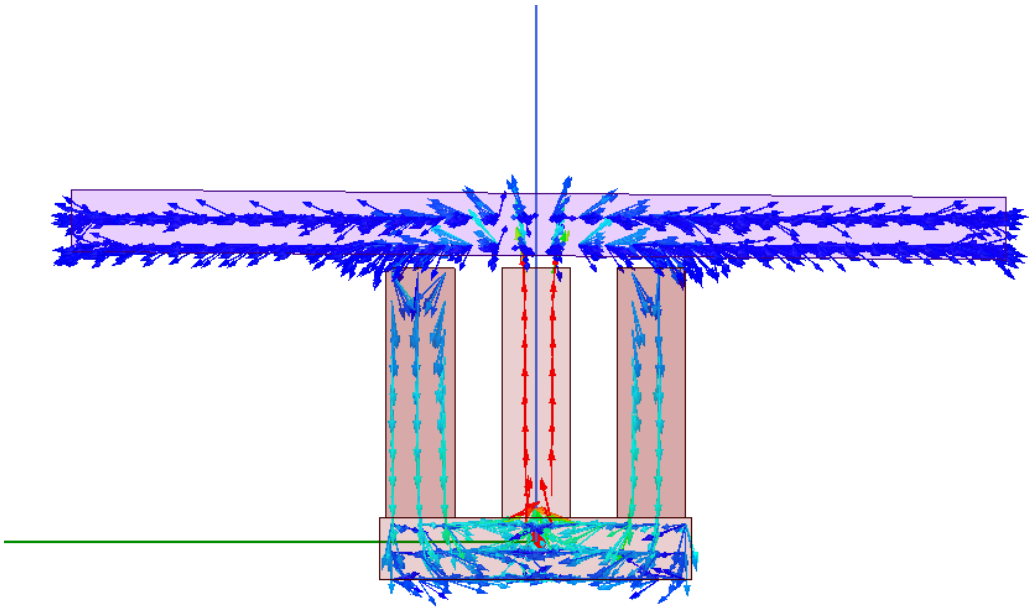


Figure 2.11 Magnetic flux distribution, side view

The analysis solved for 1 us with 100 ns step size and results are shown in the following figures;

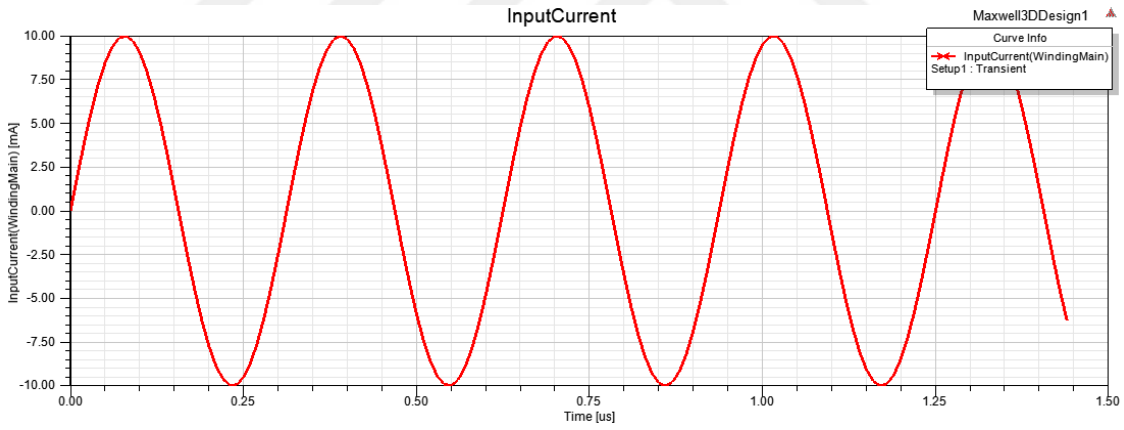


Figure 2.12 Excitation current

Figure 2.13 shows the induced voltage change against linear displacement of target. It shows nonlinear behaviours as found in analytical solution.

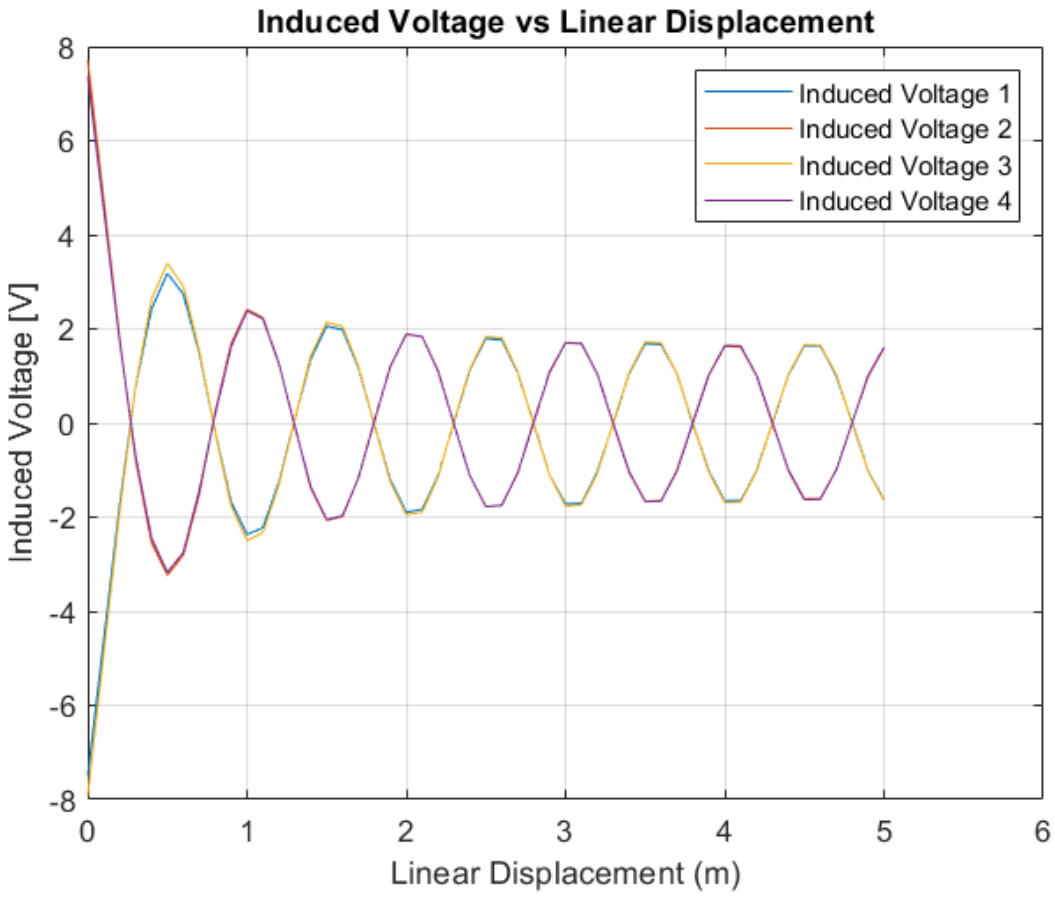


Figure 2.13 FEA result, induced voltage vs linear displacement

Figure 2.14 and Figure 2.15 show comparison of the results between analytical and FEA results. It can be seen that there is difference between analytical and FEA results. In analytical results the mechanical instabilities, eddy current losses and other losses to environment doesn't considered and that caused that difference between these results which is expected.

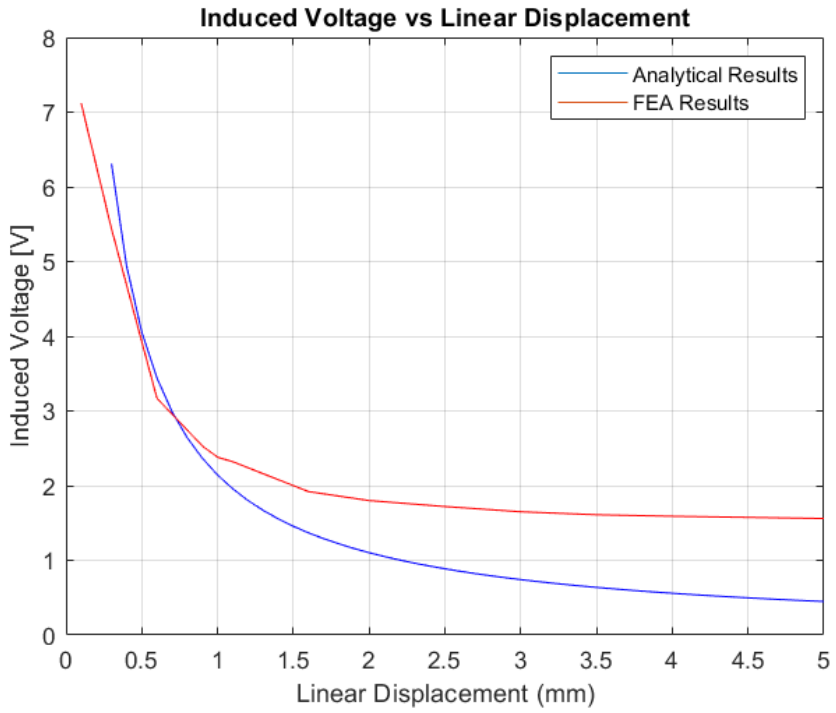


Figure 2.14 Comparison of FEA and analytical results, induced voltage vs linear displacement

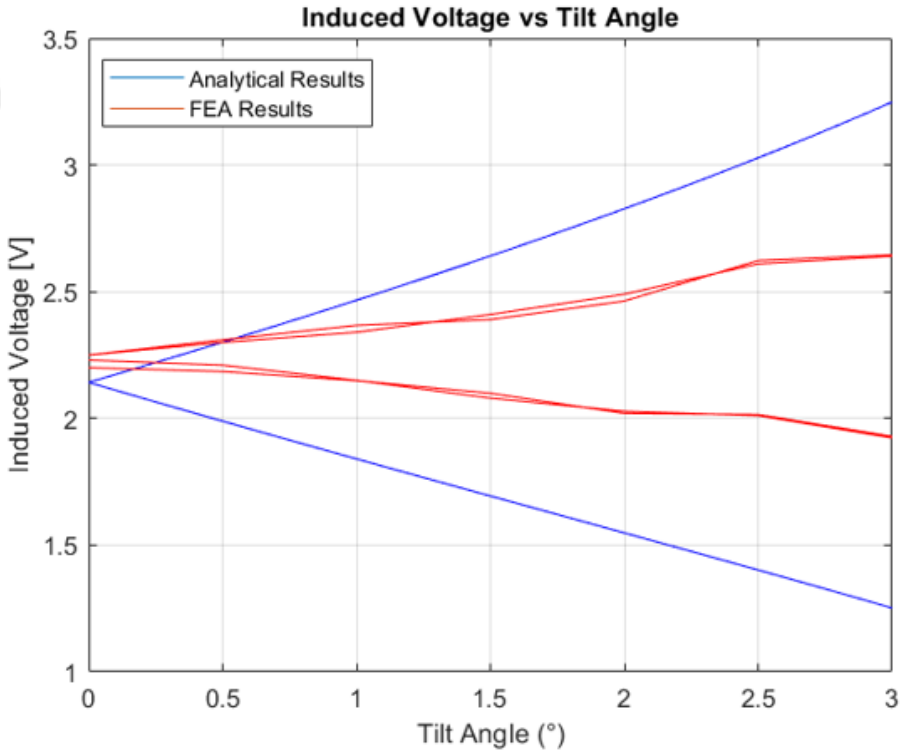


Figure 2.15 Comparison of FEA and analytical results, induced voltage vs tilt angle

3
Experimental Setup

In this section experimental setup is presented. At first a sensor is built which has similar structure used in the analysis. The sensor structure built in for experimental tests has an excitation coil in the middle and four sensing coils around it.

In analytical and FEA analysis sensor core material considered as Somalloy Soft Magnetic Material. However, because of the material's structure, it was problematic to machine it for small dimensions. Because of this, sensor core material changed as AISI 430F stainless steel which has similar magnetic characteristics with Somalloy Soft Magnetic Material.



Figure 3.1 Sensor core AISI 430F stainless steel

Dimensions of the excitation coil is 5x5x20mm, dimensions sensing coils are 5x5x20mm. Total length of the sensor is 22x22mm and all coils have turns between 35-36.

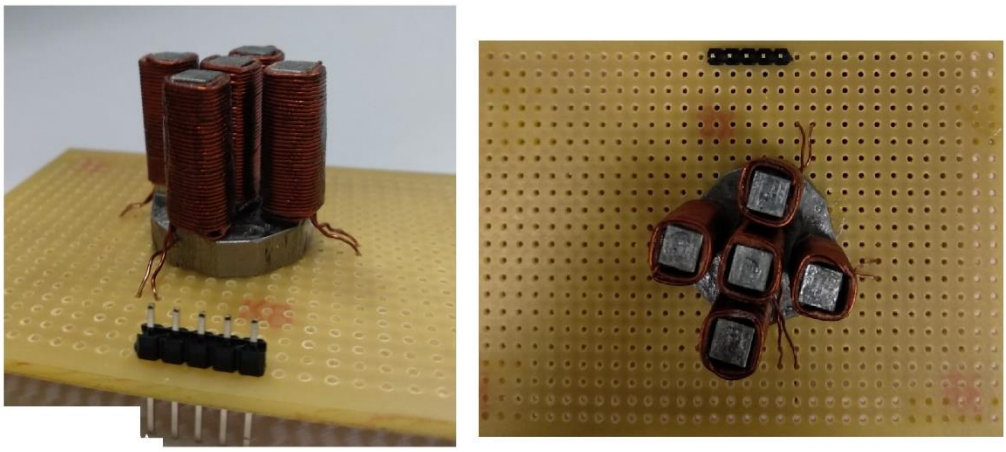


Figure 3.2 The sensor built for experimental tests

By using this sensor structure experimental tests are performed. Gauge tester which has 0.1mm and 0.2mm thickness is used to measure the displacement.

A function generator is used as an excitation source and an oscilloscope is used to measure the voltage changes on sensing coils.

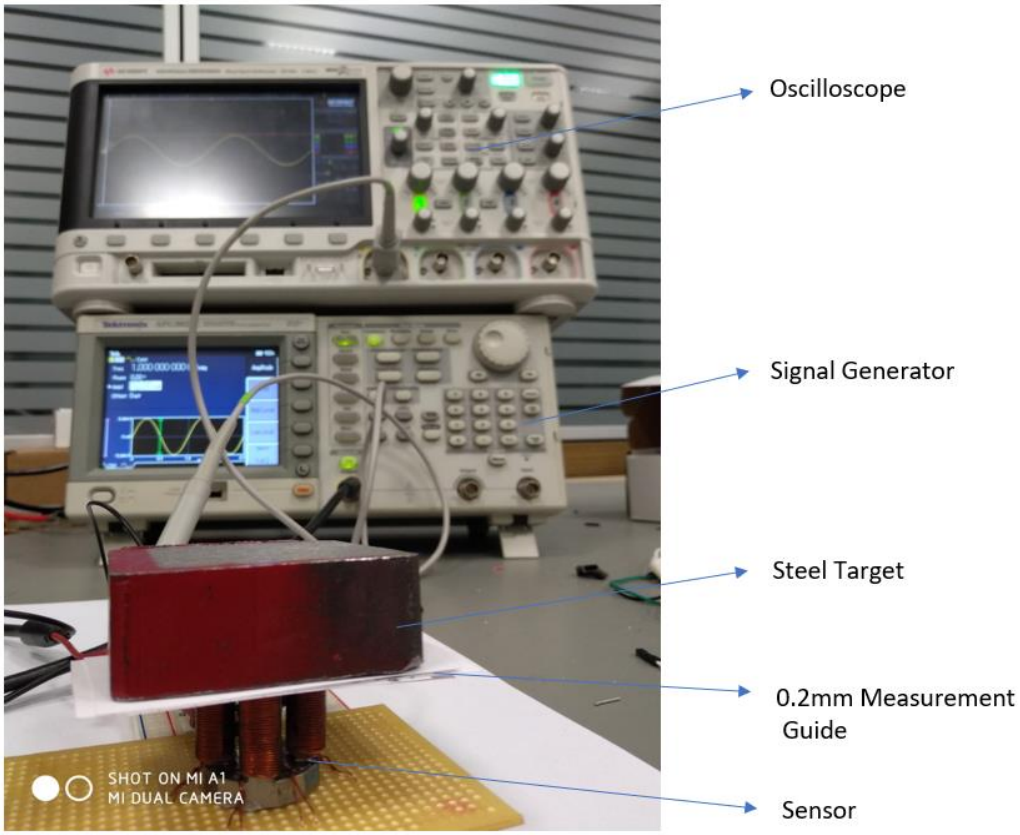


Figure 3.3 Experimental setup

Experimental tests are performed for the parameters listed in the Table 3.1;

Table 3.1 The built sensor parameters

Parameter	Magnitude	Unit
l_c	0.018	m
l_b	0.018	m
l_t	0.018	m
μ_0	4xπx10-7	-
μ_{rc}	1800	-
μ_{rb}	1800	-
μ_{rt}	450	-

3.1 Test Results

In this section a detailed results of test results are presented. Parameters listed in the Table 3.2 are used for tests.

Table 3.2 Test parameters

Parameter	Magnitude	Unit
V (excitation voltage)	10	V
f (excitation frequency)	1	MHz
N (number of turns)	35-36	-
z (linear displacement)	0-5	mm
α (tilt angle thorough x axis)	0-6	°

It can be seen from the Figure 3.4 that the built sensor shows almost linear characteristics between from 0-5mm. And Figure 3.6 shows that voltage change against tilt on sensing coils are also almost linear up to 6°.

For linear displacement measurement gauge testers which has 0.1 and 0.2mm thickness, are used. At first excitation coil is excited with a function generator and measurements are performed from sensing coils without any target material on the sensor by

oscilloscope. And then 0.1 and 0.2mm gauge testers added between the sensor and target material and measurements are performed again. This cycle kept till the 5mm linear displacement is achieved. And results are listed in the Table 3.3 and illustrated in Figure 3.4. It can be seen from the Table 3.3 that the sensor resolution is around 0.2 mm. And from Figure 3.4., we can see that the sensor has linear characteristics. The reason of the difference of measured voltage between sensing coils is the mechanical instabilities which is caused by manufacturing problems. These can be listed as the difference of number of turns on each coil, difference on measurement are of the sensing coils etc.

Table 3.3 Test results, induced voltage (peak to peak) vs linear displacement

1MHz / 10V				
	Coil 1	**Coil 2**	**Coil 3**	**Coil 4**
Distance (mm)	**Peak to Peak (mV)**	**Peak to Peak (mV)**	**Peak to Peak (mV)**	**Peak to Peak (mV)**
No Target	348	348	360	344
0	440	444	448	424
0.2	436	440	442	420
0.4	436	440	442	420
0.6	432	436	440	420
0.8	430	432	438	416
1	428	430	436	414
1.2	424	428	434	412
1.4	422	424	432	410
1.6	420	422	430	408
1.8	418	420	428	406
2	416	418	426	404
3	400	410	416	396
4	392	402	410	392
5	384	396	402	380

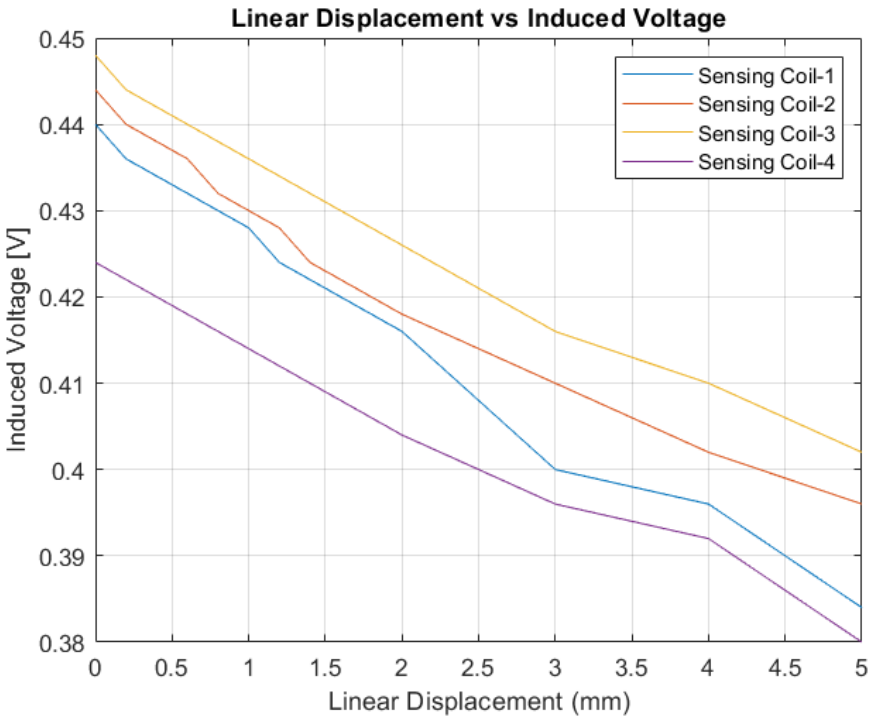


Figure 3.4 Test results, induced voltage vs linear displacement

Figure 3.6 and Table 3.4 show the induced voltage on sensing coils against tilt angle change on each coil separately. While performing tilt angle measurement, one side of the target kept fix as seen in Figure 3.5 and voltage change on sensing coils were measured. So, while the voltage on one of the sensing coils is decreasing other didn't change. And the results also show the same characteristics with linear displacement results.

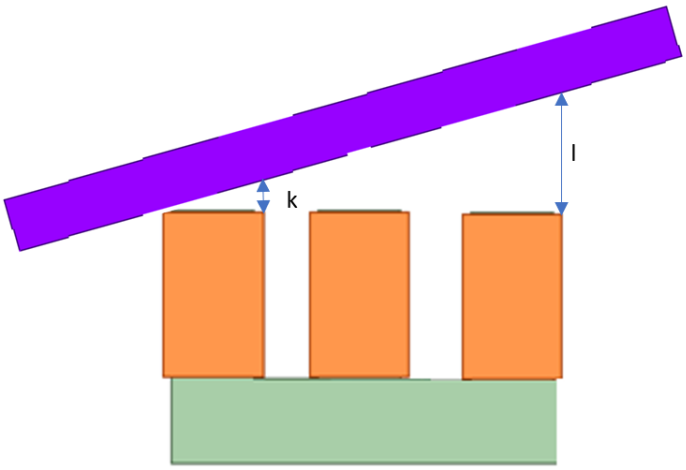


Figure 3.5 Tilt change of target, exaggerated illustration

Table 3.4 Test results, induced voltage (peak to peak) vs tilt angle

1MHz / 10V				
	Coil 1	**Coil 2**	**Coil 3**	**Coil 4**
Angle (°)	**Peak to Peak (mV)**	**Peak to Peak (mV)**	**Peak to Peak (mV)**	**Peak to Peak (mV)**
0.63	436	452	448	420
1.27	436	450	446	420
1.9	436	448	444	420
2.53	436	446	442	420
3.17	436	444	440	420
3.8	436	440	438	420
4.43	436	436	432	420
5.06	436	434	430	420
5.69	436	432	426	420

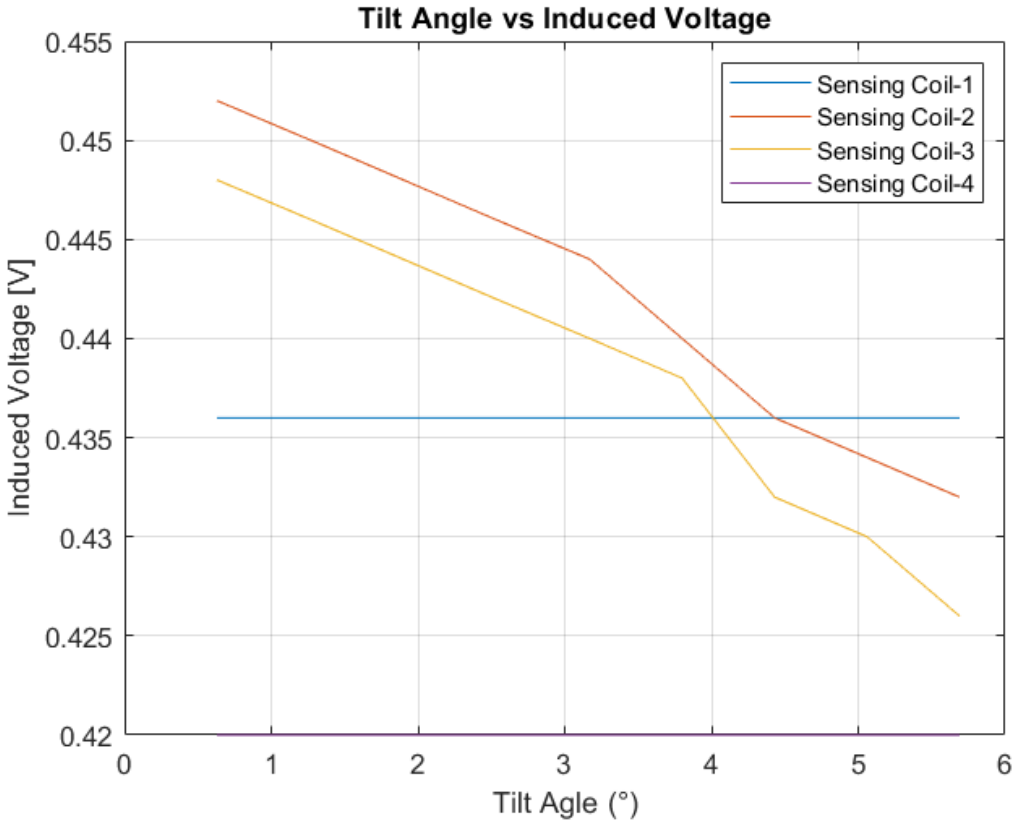


Figure 3.6 Test results, induced voltage vs tilt angle

4
Results and Discussion

In this study a novel multi axis inductive displacement sensor analysis is performed and tests are run by building the sensor. The sensor is analysed by analytically and FEA. Soft magnetic materials are chosen as a sensor core because of their magnetic characteristics. Somalloy material used for FEA and analytic results. Somalloy is produced by powder metallurgy and its really difficult to machine this material for small sizes. Because of that 430F stainless steel used for experimental setup.

The analytic and FEA results show that the voltage output can be linearized for 0-1.5 mm linear displacement and for 1.5° to 3° tilt angle. However, test results show that the built sensor has linear characteristic for 0-5mm linear displacement and 0-6° tilt angle measurement. And sensor resolution is 0.2mm linear for linear displacement and 0.6° for tilt angle measurement. The difference between sensor material and size and mechanical instabilities caused by manufacturing of the sensor, caused to occur this difference between the results.

The produced sensor can be used in harsh environments to measure linear displacement and detect the metal targets position in three dimensions. And the benefits of the sensor can be listed as follows;

- Robust and accurate measurement in harsh environment.
- Linear displacement and tilt angle measurement combined in one sensor.
- Cost effective

Beyond above advantages, the sensor has some restrictions;

- Low resolution.
- Low range.
- It can only detect metal targets.

It can be seen from the analytic and FEA results a sensor which has much better resolution can be built. To do so industrial methods can be used to produce the sensor and an IC can be designed to eliminate external effects. For much better and cost-effective sensor, a

PCB based design can be developed. This kind of design eliminates most of the external disturbances, offers a compact sensor structure and lowers the cost thanks to developed manufacturing methods.

APPENDIX A

MATLAB MODEL

Permeance Calculation

```
clc
clear all

u0 = 4*pi*(1e-7); % magnetic permeability of the core
N = 49;           % number of turns
f = 1000000;      % Excitation frequency, Hz
w = 2*pi*f;


a = 6.5e-3;
b = 12e-3;

l = -2.75e-3;
k = 2.75e-3;

z =0.3e-3:0.1e-3:5e-3; % Linear displacement, m, set 1e-3
for tilt angle calculations
alpha = 0;             % angular displacement, x axis, deg,
set 0:0.1:3 for tilt angle calculations
beta = 0;              % angular displacement, y axis, deg,
kept 0 for tilt angle calculations

Pgap1=zeros(numel(alpha),numel(beta),numel(z));
Pgap2=zeros(numel(alpha),numel(beta),numel(z));
Pgap3=zeros(numel(alpha),numel(beta),numel(z));
Pgap4=zeros(numel(alpha),numel(beta),numel(z));
PgapMain=zeros(numel(alpha),numel(beta),numel(z));

%Permeance calculation

for z1=1:numel(z)
    for alpha1 = 1:numel(alpha)
        for beta1 = 1:numel(beta)

            Pgap1(alpha1,beta1,z1) =integral2(@(x,y)
u0./(z(z1)-y*tand(beta(beta1))+x*tand(alpha(alpha1))),-b,-
a,a,b);
```

```
            Pgap2(alpha1,beta1,z1) =integral2(@(x,y)
u0./(z(z1)-y*tand(beta(beta1))+x*tand(alpha(alpha1))),-b,-
a,-b,-a);

            Pgap3(alpha1,beta1,z1) =integral2(@(x,y)
u0./(z(z1)-y*tand(beta(beta1))+x*tand(alpha(alpha1))),a,b,-
b,-a);

            Pgap4(alpha1,beta1,z1) =integral2(@(x,y)
u0./(z(z1)-
y*tand(beta(beta1))+x*tand(alpha(alpha1))),a,b,a,b);

            PgapMain(alpha1,beta1,z1) = integral2(@(x,y)
u0./(z(z1)-
y*tand(beta(beta1))+x*tand(alpha(alpha1))),l,k,l,k);

        end
    end
end
```

Equivalent Circuit Analysis

```
clc

A = 10e-3; % Excitation current, 10 mA

%Coil reluctance parameters

lc = 20e-3;          %displacement from target,m
urc = 430;           %magnetic permeability of the core,
somalloy
Ac = 5.5*5.5*1e-6;   %cross section area of the core, m

%Core reluctance parameters

lb = 22e-3;
urb = 430;
Ab = 5*25*1e-6;

%Target reluctance parameters

lt = 22e-3;
urt = 100;
At = 5*25*1e-6;

%Reluctance calculation

RC = lc/(u0*urc*Ac);     % Coil reluctance
RB = lb/(u0*urb*Ab);     % Core reluctance
RT = lt/(u0*urt*At);     % Target reluctance

%Equivalent reluctance calculation

for i = 1:1:48

    Rmain(i) = 1/PgapMain(1,1,i);
    RG1(i) = 1/Pgap1(1,1,i);
    RG2(i) = 1/Pgap2(1,1,i);
    RG3(i) = 1/Pgap3(1,1,i);
    RG4(i) = 1/Pgap4(1,1,i);

    R(i) = (Rmain(i)+RC);
    R1(i) = RG1(i)+RC+RB+RT;
    R2(i) = RG2(i)+RC+RB+RT;
    R3(i) = RG3(i)+RC+RB+RT;
    R4(i) = RG4(i)+RC+RB+RT;
```

```
    Req(i) =
R(i)+(1/((1/R1(i))+(1/R2(i))+(1/R3(i))+(1/R4(i))));

% Simplification for simulink model

    R11(i) =
(1/(1/R2(i)+1/R3(i)+1/R4(i)))/(R1(i)+(1/(1/R2(i)+1/R3(i)+1/
R4(i))));

     R22(i) =
(1/(1/R1(i)+1/R3(i)+1/R4(i)))/(R2(i)+(1/(1/R1(i)+1/R3(i)+1/
R4(i))));

      R33(i) =
(1/(1/R1(i)+1/R2(i)+1/R4(i)))/(R3(i)+(1/(1/R1(i)+1/R2(i)+1/
R4(i))));

     R44(i) =
(1/(1/R1(i)+1/R2(i)+1/R3(i)))/(R4(i)+(1/(1/R1(i)+1/R2(i)+1/
R3(i))));

    % Induced voltage calculation in Simulink
    sim('ResultsAnaliticFourCoilModel_2016b_v5');

    Maxx1(i) = max(Results1);
    Maxx2(i) = max(Results2);
    Maxx3(i) = max(Results3);
    Maxx4(i) = max(Results4);
End
```

Results

```
figure(1)

t = 0:0.1:4.9;

plot(z,Maxx1);
hold on
plot(z,Maxx2);
hold on
plot(z,Maxx3);
hold on
plot(z,Maxx4);

grid on

title('Induced Voltage vs Linear Displacement')
xlabel('Linear Displacement (m)')
%xlabel('Tilt Angle (°)')
ylabel('Induced Voltage [V]')
legend({'Induced Voltage 1','Induced Voltage 2','Induced
Voltage 3','Induced Voltage 4'})

figure(2)

plot(z,R11);
hold on

figure(3)
plot(z,Req);
title('Equivalent Reluctance vs Linear Displacement');
xlabel('Linear Displacement (m)')
ylabel('Equavalent Reluctance [At/Wb]')

grid on
```

Simulink Model

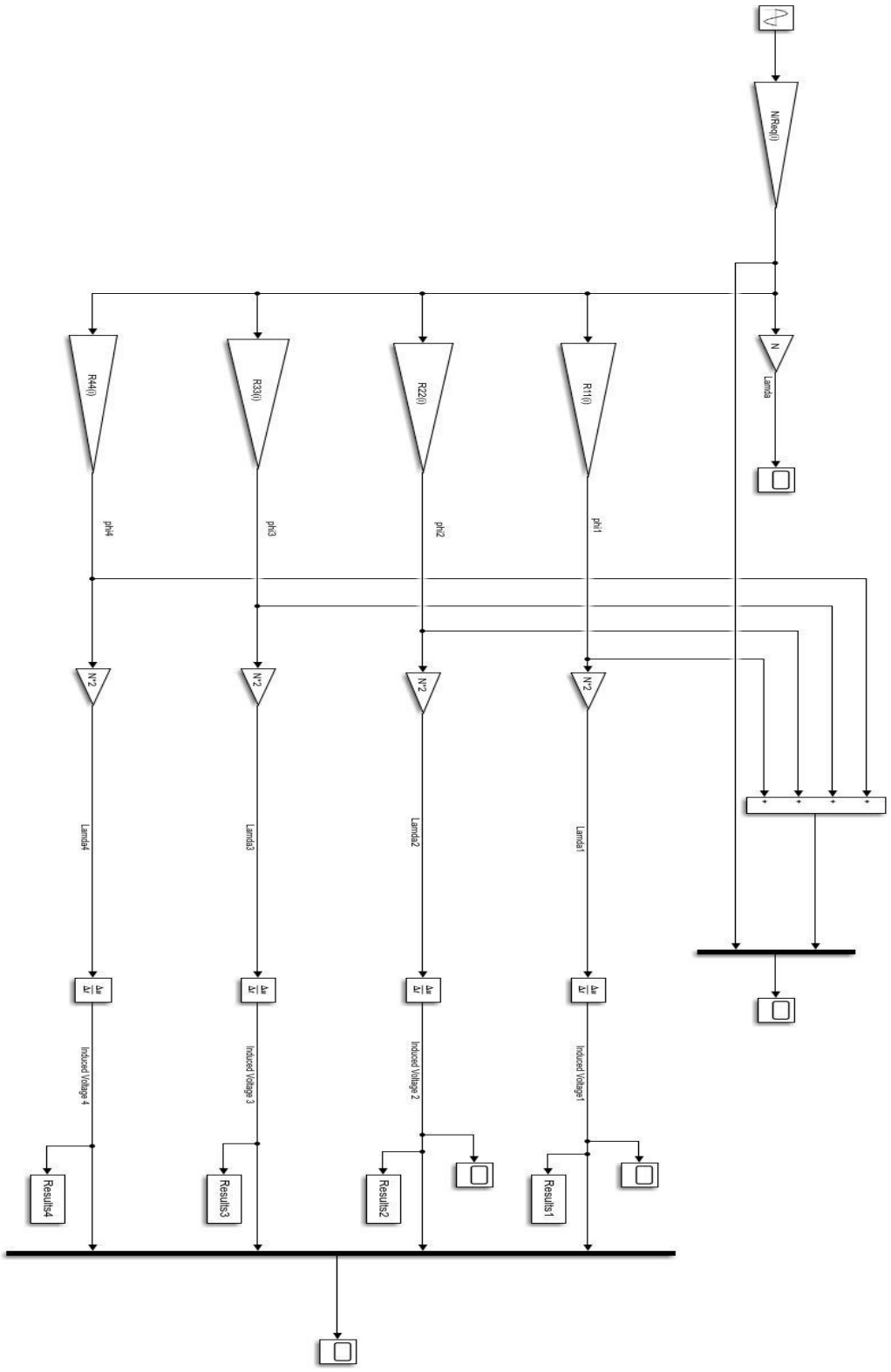


Figure A.1 Simulink model of equivalent circuit

APPENDIX B

CarTech® 430F Solenoid Quality Stainless

Table B.1 430F material properties

Carbon (Maximum)	0.07 %	**Manganese (Maximum)**	0.80 %
Phosphorus (Maximum)	0.030 %	**Sulfur**	0.250 to 0.400 %
Silicon	0.30 to 0.70 %	**Chromium**	17.25 to 18.25 %
Nickel (Maximum)	0.60 %	**Molybdenum (Maximum)**	0.50 %
Iron	Balance		

Description

CarTech 430F Solenoid Quality Stainless is a ferritic chromium-iron stainless alloy, the chemical composition and processing of which are controlled within precise limits to assure consistently high magnetic permeability, low coercive force (HC) and low residual induction (Br), while offering corrosion resistance similar to that of standard CarTech 430F stainless.

Applications

CarTech 430F Solenoid Quality Stainless has been specifically developed for use in soft magnetic components which must operate in corrosive environments.

Magnetic Properties

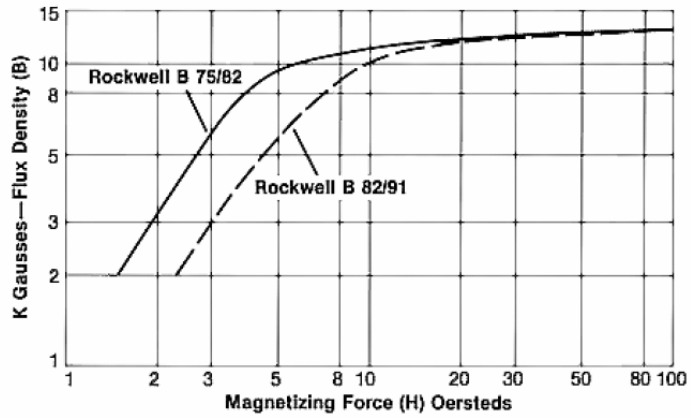


Figure B.1 Magnetic properties

Somaloy ® Prototyping Material, SPM

General	
Base material: Somaloy Prototyping Material	Somaloy Prototyping Material blanks exhibit stable mechanical properties up to 150ºC

Mechanical properties			Standards
Transverse rupture strength/150ºC	[MPa]	60/60	SS-ISO 3325
Tensile strength	[MPa]	15*	SS-EN 10002-1, ISO
Yield strength	[MPa]	5*	SS-EN 10002-1, ISO
Young's modulus	[GPa]	100*	ASTM E 1876-99
Poisson's ratio	–	0.23	ASTM E 1876-99
Impact Energy	[J]	1.3	SS-EN 10045, SS-EN

* The machining quality may influence the expected mechanical strength.

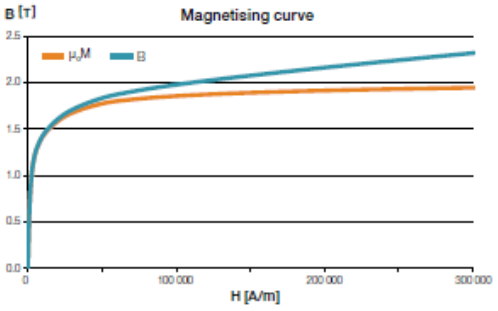
Physical properties			Standards
Density	[g/cm³]	7.3	SS-ISO 2738
Thermal expansion	[K⁻¹]	11 e-06	ASTM E 228/MPIF 35
Resistivity	[µΩm]	300	Four point measurements on nominal size OD 55mm ID 45mm Height 5mm

Magnetic properties			Standards
B@4000A/m	[T]	1.19	IEC 60404-4
B@10000A/m	[T]	1.46	IEC 60404-4
H_c	[A/m]	210	IEC 60404-4
μ_r-max	–	430	IEC 60404-4

Available blanks	Size
Cylindrical	OD 80/H20 mm
Cylindrical	OD 80/H40 mm
Cylindrical	OD 120/H20 mm
Ring	OD155/ID105/H20 mm

Magnetising curve

Data adjusted for use in Finite Element Modeling.



H[A/m]	μ_0M[T]	B[T]	H[A/m]	μ_0M[T]	B[T]
0	0.00	0.00	12904	1.47	1.49
93	0.03	0.03	26799	1.65	1.68
165	0.06	0.06	49770	1.77	1.83
284	0.13	0.12	74770	1.82	1.92
399	0.19	0.19	99770	1.85	1.98
457	0.23	0.23	124770	1.87	2.03
1104	0.58	0.58	149770	1.89	2.08
1594	0.77	0.77	189770	1.91	2.15
2306	0.94	0.95	229770	1.92	2.21
3606	1.12	1.13	279770	1.93	2.29
6468	1.30	1.31	304770	1.94	2.33

Core loss

[W/kg]	50/60 Hz	100 Hz	200 Hz	300 Hz	400 Hz	500 Hz	600 Hz	700 Hz	800 Hz	900 Hz	1000 Hz	2000 Hz
0.5T	1.6 / 1.9	3.1	6	10	14	17	21	26	30	34	39	95
1.0T	5.2 / 6.3	11	22	34	47	60	74	88	104	120	136	339
1.5T	11 / 13	22	45	70	96	123	153	183	216	249	284	719

Measured according to CEI/IEC 60404-6:2003 on ring sample (OD55 ID45 H5 mm).

Figure B.2 Somalloy material properties

APPENDIX C

Produced Sensor Core Manufacturing Document and Dimensions

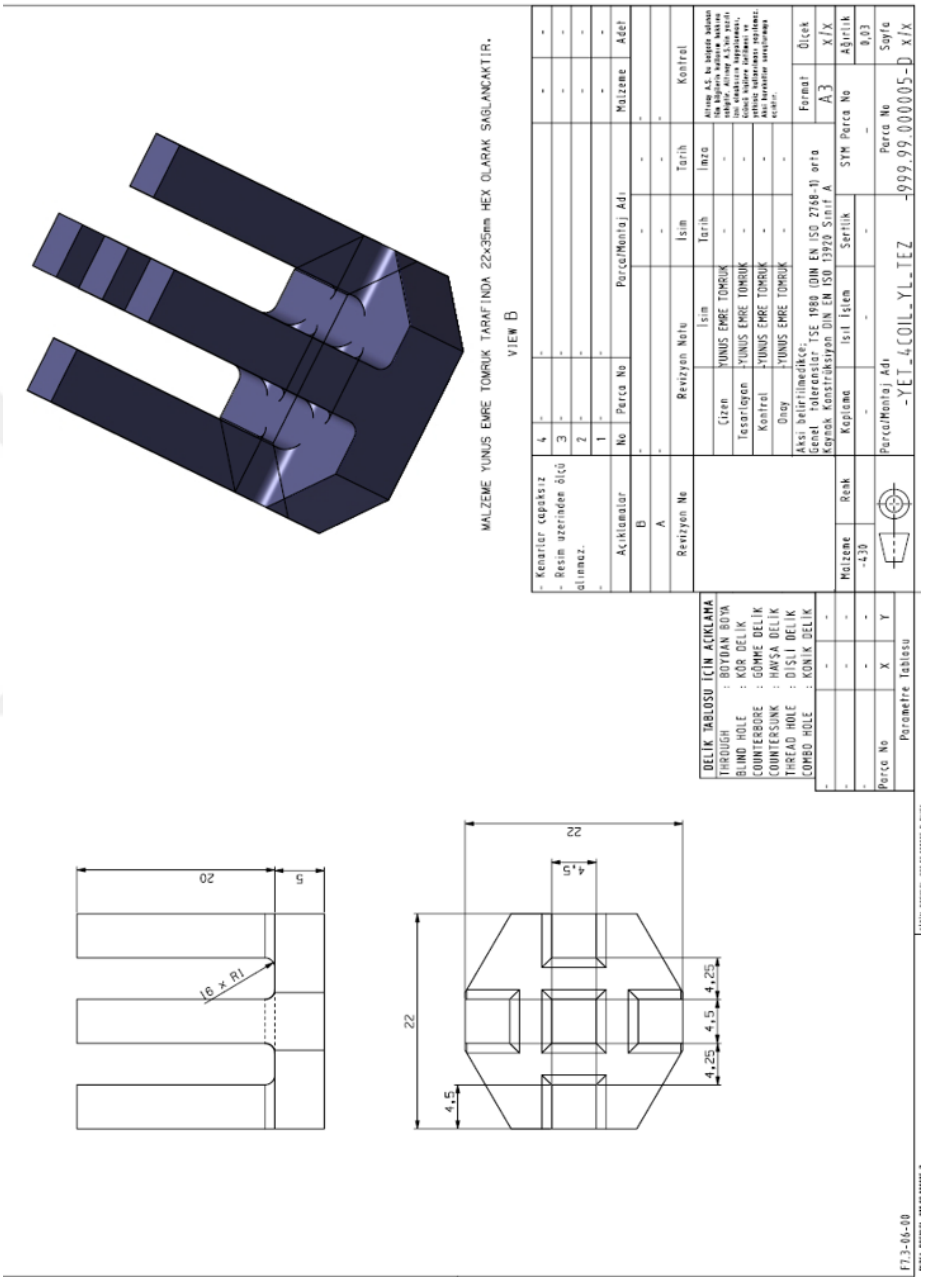


Figure C.1 Sensor core technical drawing

References

[1] Kaman Precısıon Products, “Inductıve technology handbook”, 2012

[2] M. R. Nabavi, “Low-power high-performance integrated interface for eddy-current displacement sensors”,Phd Thesis, 2011

[3] B. George, Tan. Z and S. Nihtianov. "Advances in capacitive, eddy current and magnetic displacement sensors and corresponding interfaces." IEEE Trans. Ind. Electron 64 2017, pp. 9595-9607.

[4] S. Tumanski, “Induction coil sensors—A review” Measurement Science & Technology – vol. 18, no. 3, 2007.

[5] M. R. Nabavi and S. Nihtianov, “Design Strategies for Eddy-Current Displacement Sensor Systems: Review and Recommendations”, IEEE Sensors Journal, vol. 12, no. 12, 2012, pp. 3346-3355.

[6] K Wang, L Zhang, Y Le, S Zheng, B Han and J. Yiang, “Optimized differential self-inductance displacement sensor for magnetic bearings: Design analysis and experiment”, IEEE Sensors Jou.., vol. 17, no. 14, 2017, pp. 4378-4387.

[7] Z. Kokolanski, J. Jordana, M. Gasulla, V. Dimcev and. "Direct inductive sensor to microcontroller interface circuit." Sensors and Actuators A: Physical, vol. 224, 2015, pp. 185-191.

[8] M. R. Nabavi and S. Nihtianov, “Eddy-Current Sensor Interface for Advanced Industrial Applications”, Industrial Electronics, IEEE Transactions, vol. 58, no.9, 2011, pp 4414-4423.

[9] R. Olaru, and D. Dragoi, “Inductive tilt sensor with magnets and magnetic fluid”, Sensors and Actuators A: Physical, vol. 120, 2005.

[10] L. Rovati and S. Cattini, ”Contactless Two-Axis Inclination Measurement System Using Planar Flux-Gate Sensor”, IEEE Trans. Instrumentation and Measure, vol. 59, no. 5, 2010, pp. 1284-1293.

[11] Z. Zhang, F.L. Ni, Y. Dong, J. Minghe, H. Liu,”A novel absolute angular position sensor based on electromagnetism”, Sensors and Actuators A: Physical, vol. 194, 2013, pp. 196-203.

[12] S. C. Chen, D. K. Le and V. S. Nguyen. "Inductive displacement sensors with a notch filter for an active magnetic bearing system." Sensors 14.7 2014, pp. 12640-12657.

[13] S Fericean and R Droxler “New noncontacting inductive analog proximity and inductive linear displacement sensors for industrial automation”, IEEE Sensors Jou., vol. 7, no. 11, 2007, pp. 1538-1545.

[14] Ragunathan, P & Edeswaran, Logashanmugam. “Design and Fabrication of Low Cost Eddy Current Sensor for Position Control Applications.” Indian Journal of Science and Technology. 9. 10.17485/ijst/2016/v9i42/104645.

[15] B. Anish and G.Boby. “ Design and Development of a New Non-Contact Inductive Displacement Sensor.” IEEE Sensors Journal. PP. 1-1. 10.1109/JSEN.2017.2780835, 2016.

[16] O. Sosnicki, G. Michaud, F. Claeyssen. “Eddy Current Sensors on Printed Circuit Board for Compact Mechatronic Application.” Sensoren und Messsysteme 2010 - 15. ITG/GMA-Fachtagung

[17] Chen, Seng & Kha, Le & Sum, Nguyen. “ Inductive Displacement Sensors with a Notch Filter for an Active Magnetic Bearing System. Sensors.” 2014, (Basel, Switzerland). 14. 12640-12657. 10.3390/s140712640.

[18] R. Luigi and C. Stefano. “ Contactless Two-Axis Inclination Measurement System Using Planar Flux-Gate Sensor.” 2010, Instrumentation and Measurement, IEEE Transactions on. 59. 1284 - 1293. 10.1109/TIM.2010.2040908.

[19] P. Reddy, Battu and Murali, Ashwin and Shaga, Ganesh. “ Low cost planar coil structure for inductive sensors to measure absolute angular position.”, 2017, 14-18. 10.1109/ICFST.2017.8210463.

[20] Grobler, A.J. & Schoor, George & Ranft, E.O.. “ Design and Optimisation of a PCB Eddy Current Displacement Sensor.” 2017, SAIEE Africa Research Journal. 108. 4-11. 10.23919/SAIEE.2017.8531511.

Publications from the thesis

Contact Information: yetomruk@gmail.com

Conference Papers

1. Tomruk Y.E., Güney Ö.F. , Erkan K. , "A Novel Multi Axis Inductive Displacement Sensor Design and Analysis", Ereğli International Science and Academic Congress Proceedings Book, ISBN:978-605-7852-54-0, Volume 3, 22-23